Laser Optoacoustic Imaging for Breast Cancer Diagnostics: Limit of Detection and Comparison with X-ray and Ultrasound Imaging

Rinat O. Esenaliev[1], Alexander A. Karabutov[1], Frank K. Tittel[1],
Bruno D. Fornage[2], Sharon L. Thomsen[2], Carol Stelling[2], and Alexander A. Oraevsky[1]

[1] Department of Electrical and Computer Engineering, Rice University, Houston TX 77005
[2] Department of Diagnostic Radiology, UT / M.D. Anderson Cancer Center, Houston, TX 77030

ABSTRACT

Laser optoacoustic imaging is a promising diagnostic technique for early breast cancer detection. Capability of laser optoacoustic imaging for visualization of small spherical tumor phantoms located within the bulk collagen gels was studied. The experiments were performed with breast phantoms made of optically turbid collagen gel. Optical properties of the phantom resembled the optical properties of human breast at the wavelength of irradiation, 1064 nm (μ_a=0.11 1/cm, μ_s'=2.92 1/cm). Gel spheres with a higher absorption coefficient, μ_V=0.75 1/cm were used to simulate tumors. The experiments demonstrated the capability of laser optoacoustic imaging to detect and localize 2-mm "tumors" at a depth of up to 60 mm within 100-mm thick breast phantoms. Laser optoacoustic images of the phantom tumors were reconstructed from experimentally measured pressure profiles. The optoacoustic images were compared with images obtained with x-ray mammography and ultrasonography. Comparative study revealed experimental conditions and phantom structure for which the laser optoacoustic imaging outperformed both the x-ray mammography and the ultrasonography. The results suggest that the laser optoacoustic imaging may occupy an important niche in breast cancer diagnostics, particularly, for diagnosis of small tumors in radiologically dense and acoustically homogeneous breast tissues.

1. INTRODUCTION

X-ray mammography and ultrasonography are the two major imaging techniques currently applied in breast cancer diagnostics. These techniques are not free from serious limitations. X-ray imaging fails to detect tumors in radiologically dense tissues. Ultrasonography is not capable to detect tumors with acoustic properties similar to those of normal breast tissue. Various types of optical tomography have been proposed for cancer diagnostics and intensively developed during the last decade (see, for example, the SPIE and OSA proceedings [1,2]. Optical tomography is based on differences in optical properties between tumor and normal tissues. The difference in absorption coefficient can result from higher blood content in malignant tumors in comparison with normal tissues [3], which in turn is associated with increased vascularization in rapidly growing tumors [4,5]. Since hemoglobin of blood is the major chromophore in biological tissues in the visible and near infra-red spectral range [6,7], malignant tumors may have higher absorption coefficient than normal tissues. In addition, cancer cells are known to accumulate increased concentration of porphyrins that may absorb near-IR light. Recent clinical studies that employed optical imaging techniques confirmed existence of optical contrast between normal and cancerous tissues in the breast [8,9]. However, strong light scattering and attenuation in biological tissues substantially limit capabilities of optical tomography.

Several years ago, the time-resolved laser optoacoustic technique was proposed for imaging in biological tissues [10]. Laser optoacoustic tomography in transmission mode (LOAT-T) utilizes acoustic signals induced by laser pulses in tumors and transmitted to the acoustic transducer along the axis of laser irradiation [11-13]. LOAT-T combines advantages of optical excitation with acoustic detection and, therefore, overcomes the problem associated with strong light scattering in biological tissues [14-16]. Laser optoacoustic tomography utilizes optical contrast and detection of laser-induced acoustic waves. The profiles of acoustic waves generated under irradiation conditions of temporal pressure confinement in the volume of tumors, resemble the profile of absorbed laser energy [10]. Tumors with dimensions from 1 mm to 10 mm irradiated with laser pulses represent themselves as sources of acoustic waves with ultrasonic frequencies of 150 kHz to 1.5 MHz. Such ultrasonic waves can propagate in bio-tissues with insignificant attenuation [16]. However, acoustic diffraction in the ultrasonic frequency range $\leq$ 1 MHz is pronounced and must be compensated upon detection [17,18].

The objectives of the present study were: (1) to compare capabilities of the three techniques (laser optoacoustic imaging, X-ray mammography, and ultrasonography), and (2) to demonstrate reliable detection of small spherical tumors in phantoms simulating radiologically dense and acoustically homogenous breast. Limits of breast tumor detection with optoacoustic technique were also determined in the experiments presented below.

Downloaded From: http://proceedings.spiedigitallibrary.org/ on 07/11/2016 Terms of Use: http://spiedigitallibrary.org/ss/TermsOfUse.aspx

Basic equations for laser optoacoustic tomography in transmission mode. Laser optoacoustic tomography is based on generation, detection, and analysis of thermoelastic pressure waves induced by pulsed laser radiation in the volume of tissue under diagnosis [10]. The pressure distribution, P(**r**), induced under irradiation conditions of temporal stress confinement can be expressed as:

$$P(\mathbf{r}) = \Gamma(\mathbf{r})\mu_a(\mathbf{r})F(\mathbf{r}) \tag{1}$$

where $\Gamma(\mathbf{r})$ is the Grüneisen coefficient, $\mu_a(\mathbf{r})$ is the absorption coefficient, and $F(\mathbf{r})$ is the laser fluence distribution in tissue. The Grüneisen coefficient is a function of the three physical parameters: thermal expansion coefficient, β, speed of sound, c_s, and heat capacity at constant pressure, C_p:

$$\Gamma = \frac{\beta c_s^2}{C_p} \tag{2}$$

Since biological tissues are heterogeneous media, all the three parameters are functions of distance, **r**, in tissue. Therefore, the Grüneisen coefficient of biological tissues is also a function of **r**. The laser optoacoustic tomography can utilize differences in all three parameters involved in the equation (1): the absorption coefficient, the fluence distribution (which depends on tissue scattering), and the Grüneisen coefficient. Thus, laser optoacoustic imaging employs not only the optical contrast, but also the contrast in thermomechanical properties between normal and malignant tissues.

The conditions of temporal confinement of laser-induced pressure may be satisfied in 1-mm (or larger) tumors upon irradiation of breast with submicrosecond (or nanosecond) laser pulses. Let us assume that a volume, v, of malignant tissue with a linear dimension, Δz, is located at a distance, z_V, from the irradiated surface along the axis of laser irradiation (Fig. 1). The laser-induced pressure will be temporarily confined in the irradiated volume, if the duration of the laser pulse, τ_p, is shorter than the time, τ_{rel}, it takes for the pressure wave to propagate the distance, Δz, i.e.

$$\tau_p << \tau_{rel} = \Delta z / c_s \tag{3}$$

Since the speed of sound in soft biological tissues is close to the speed of sound in water (c_s = 1.5 μm/ns), laser pulses with duration of ~100 ns should be used to provide stress confinement in small tumors with dimensions of 1 mm by the order of magnitude. The pressure rise in the volume of tumor with increased absorption, $P(z_v)$, is proportionally higher than that in surrounding tissues. Assuming 1-D geometry and constant Grüneisen coefficient in the tissue, one can express $P(z_v)$ as:

$$P_V = \Gamma_V \mu_V F_V \tag{4}$$

where the Grüneisen coefficient, and the absorption coefficient in the volume of tumor are different from those in surrounding normal tissues. The laser-induced pressure pulse can propagate in all directions as a spherical acoustic wave with the center inside the tumor. The time-resolved measurements of the pressure pulse with acoustic transducers allow accurate determination of tumor dimensions and location within the volume of normal tissue. Spatial resolution is defined by the upper limit of the transducer ultrasonic bandwidth. Fig. 1 represents the schematic diagram of the laser optoacoustic tomography in transmission mode (when laser irradiation and acoustic detection performed from opposite surfaces of the breast).

The time interval, τ, between the acoustic signal induced in piezoelectric crystal by laser irradiation of the transducer and the acoustic signal induced in the volume of "tumor" depends on the distance between the "tumor" and the piezoelectric crystal, R_v:

$$R_V = c_s \tau \tag{5}$$

The values z_v and R_v relate to the total thickness of the tissue, D, as:

$$z_V = D - R_V \tag{6}$$

Downloaded From: http://proceedings.spiedigitallibrary.org/ on 07/11/2016 Terms of Use: http://spiedigitallibrary.org/ss/TermsOfUse.aspx

The pressure pulse duration, $\Delta\tau$, upon irradiation conditions of temporal stress confinement satisfies the following formula:

$$\Delta z = c_s \Delta\tau \tag{7}$$

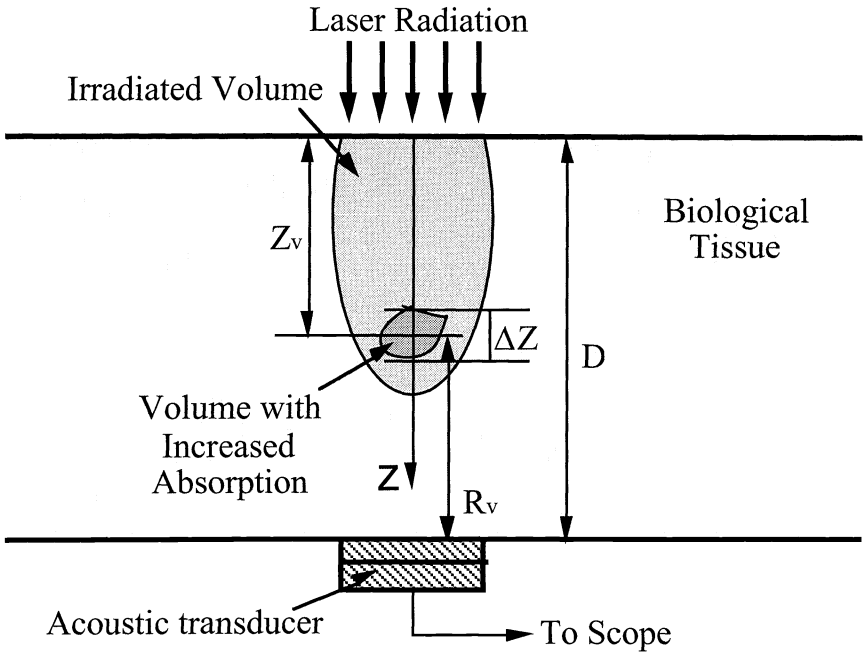

Figure 1. Generation and transmission mode detection of optoacoustic pressure waves in tissues.

Therefore, time-resolved measurements of the laser-induced pressure distribution along the z-axis yield Δz. The equations (1)-(7) utilize parameters that can be measured by acoustic transducers (absolute value of pressure waves, P, temporal characteristics τ and $\Delta\tau$), to yield the parameters of tissues under imaging (μ_a, R, Δz). Measurements of laser-induced absolute pressure provide diagnostic information for tissue characterization. Analysis of the pressure temporal profile allows image reconstruction on the basis of tissue optical (primarily) and thermoelastic properties.

Pressure profile from an absorbing sphere. The early tumors can be considered as small spheres with increased absorption coefficient. The acoustic waveform generated in a small spherical tumor and detected by a wide-band acoustic transducer at the irradiated surface can be found from the following equation [19]:

$$P(r,t) = \frac{\beta c_s}{2rC_p} \int dr'\, r' \left[H(r, t - \frac{r - r'}{c_s}) - H(r, t - \frac{r + r'}{c_s})\right] \tag{8}$$

where the simplified expression for the laser fluence of a short pulse is given by:

$$H(r,t) = \delta(t)\mu_V F_V \begin{cases} 1, r \le r_0 \\ 0, r > r_0 \end{cases} \tag{9}$$

where F_V is the effective laser irradiance in "tumor", $\delta(t)$ is the delta-function.

Downloaded From: http://proceedings.spiedigitallibrary.org/ on 07/11/2016 Terms of Use: http://spiedigitallibrary.org/ss/TermsOfUse.aspx

The analytical solution of the system (8), (9) describes the bipolar N-shaped temporal profile of optoacoustic pressure detected from an absorbing sphere in the far zone (see Fig. 2):

$$P_{sph}(\tau') = \frac{\Gamma_V}{2r}\mu_V F_V r_o (1-\tau')[\Theta_{0,1}(\tau') + \Theta_{1,2}(\tau')] \tag{10}$$

where τ' is so-called retarded time from the edge of the sphere (Fig. 2), $\Theta_{0,1}(\tau')$ is a square wave function constructed from two Heaviside functions. It is equal to 1 for values of τ' between 0 and 1, and zero, otherwise. $\Theta_{1,2}(\tau')$ is the same function, but for the values of τ' between 1 and 2.

Total duration of the N-shaped wave, τ_{sph}, is related to the sphere radius, r_0, as:

$$\tau_{sph} = \frac{2r_o}{c_s} \tag{11}$$

Amplitude of the wave, P_{sph}, decreases as 1/r with increase of the distance from the sphere:

$$P_{sph} = \frac{P_V}{2}\frac{r_o}{r} \tag{12}$$

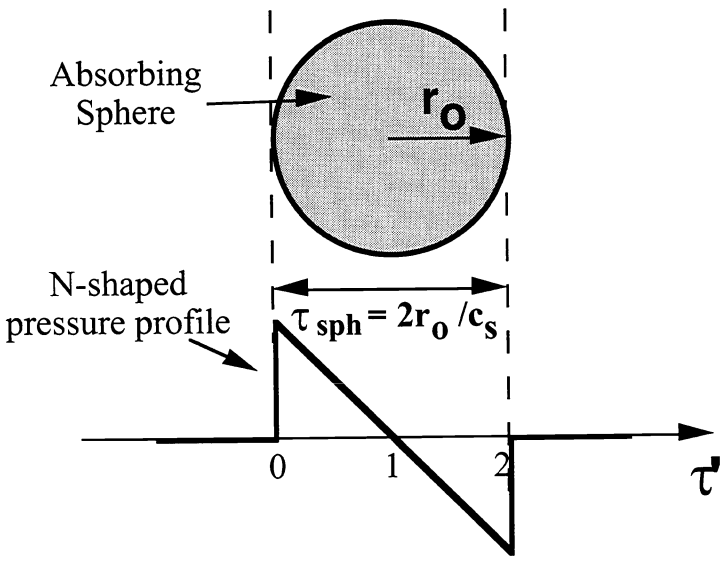

Figure 2. Temporal profile of optoacoustic pressure from an absorbing sphere.

Therefore, optoacoustic signal from a spherical tumor with increased absorption will have bipolar shape with amplitude directly proportional to the product of the Grüneisen and absorption coefficients, laser fluence, tumor radius, and inversely proportional to the distance, $R_{sph} = r$, from the tumor to the acoustic transducer:

$$P_{sph} = \frac{\Gamma_V}{2}\mu_V F_V \frac{r_o}{r} \tag{13}$$

Downloaded From: http://proceedings.spiedigitallibrary.org/ on 07/11/2016 Terms of Use: http://spiedigitallibrary.org/ss/TermsOfUse.aspx

Thus, the measurements and subsequent analysis of the acoustic signal duration, shape, and position can provide information about tumor dimensions, shape, and distances from the acoustic transducers located along the perimeter of the breast.

2. MATERIALS AND METHODS

Breast phantoms were made of 10%-gelatin and had dimensions of 100 x 97 x 57 mm (Fig. 3). Water absorption (μ_a = 0.12 cm^{-1} at 1064 nm [20]) provided the absorption coefficient of 0.11 cm^{-1} in the gel phantoms. The typical effective attenuation coefficient, μ_{eff}, for normal breast tissue *in vivo* is close to 1.0 cm^{-1} in the near-infrared spectral range [21,22]. Polystyrene spheres or milk were used, to provide effective scattering coefficient of 2.92 cm^{-1}. Absorption by water and scattering by polystyrene microspheres yielded an effective attenuation of 1.0 cm^{-1} for our phantom.

Tumor phantoms were made of the same optically turbid gel and colored with the bovine hemoglobin. The phantoms had spherical shape and absorption coefficient of 0.75 cm^{-1}. Diameter of the spheres was varied from 2 to 6 mm. The spheres were stringed on thin nylon white threads attached to a hollow plexiglas cube in order to provide their fixation inside the phantom. Liquid gel at the temperatures very close to the solidification temperature was poured inside the cube. After solidification in a refrigerator the phantom was taken out from the plexiglas cube. Thus, the breast phantoms were made acoustically homogeneous and radiologically dense, while absorption coefficients of the spheres and surrounding gel were 7 fold different.

X-ray images of the breast phantoms were obtained with the use of clinical mammography machine (General Electric, Schenectady, NY). The best contrast of x-ray images was achieved with application of molybdenum anode and molybdenum filter at the voltage of 30 kV. Ultrasonography was performed with a modern sophisticated ultrasound machine Sonoline Elegra (Siemens, New York, NY) with various contrast enhancement features. Both X-ray and ultrasound imaging machines are being applied for breast cancer diagnostics at M. D. Anderson Cancer Center.

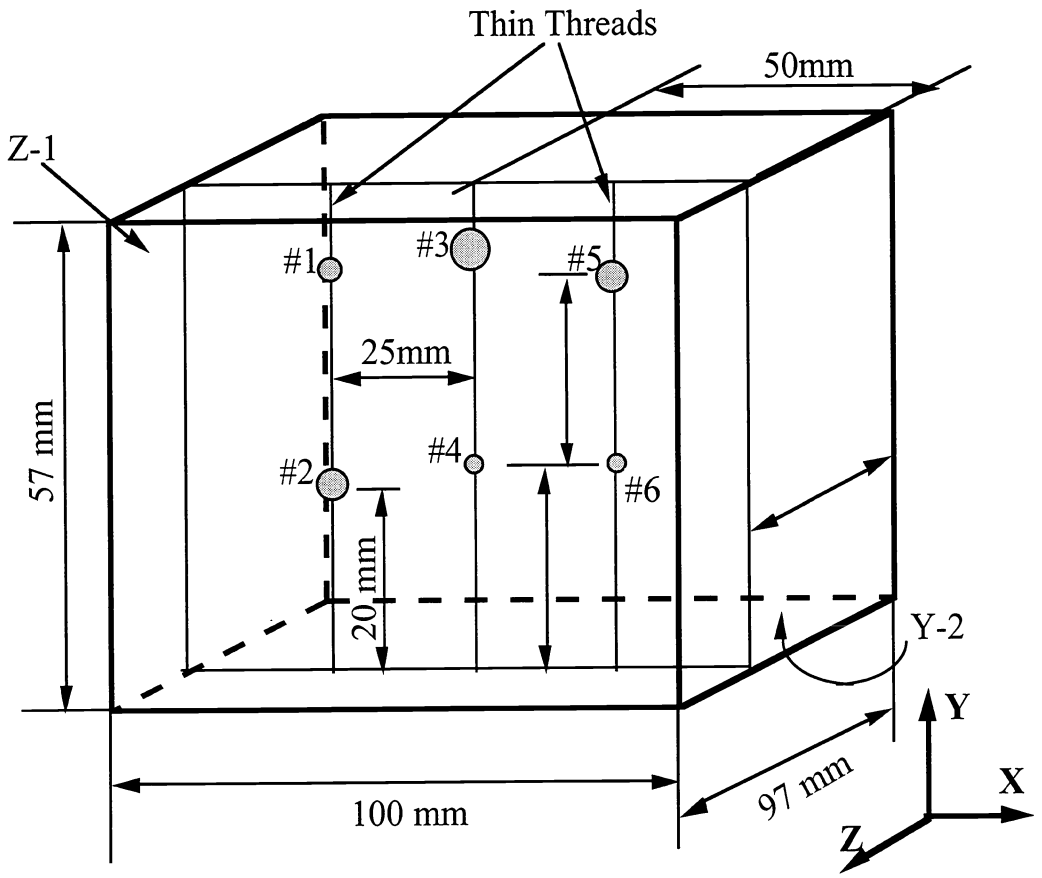

Figure. 3. 3D schematic diagram of the gelatin breast phantom with absorbing spheres simulating tumors. Diameters: 3, 4, 6, 2, 4, and 2 mm (spheres #1, 2, 3, 4, 5, and 6, respectively).

Downloaded From: http://proceedings.spiedigitallibrary.org/ on 07/11/2016 Terms of Use: http://spiedigitallibrary.org/ss/TermsOfUse.aspx

A Q-switched Nd:YAG laser was used for optoacoustic experiments. It had the following parameters: pulse duration - 14 ns, wavelength - 1064 nm, pulse energy - 100 mJ. The diameter of laser spot was 8 mm providing incident fluence of 200 mJ/cm^2.

Laser optoacoustic experiments were performed in transmission mode (Fig. 1), which is based on irradiation of the phantoms and detection of optoacoustic pressure waves from opposite sides. Specially designed sensitive acoustic transducers (LBAT-01, Science Brothers Inc., Houston, TX) with dumped internal reflections were used for detection of pressure waves from the samples. Transducer signals were acquired with the use of a digital oscilloscope and analyzed by a microcomputer. Wavelet transform was applied to denoise raw acoustic signals (to increase the signal-to-noise ratio) [23]. Optoacoustic images were created with MatLab using wavelet processed optoacoustic signals and an image reconstruction algorithm in Cartesian coordinates that rejects signals arriving to the transducer at angles deviating from laser beam - transducer axis. A simple 2D-plotting routine was employed to reconstruct images of phantom tumors. Any two series of the pressure profiles recorded upon laser irradiation of the two orthogonal surfaces of the phantoms could be employed for the 2D optoacoustic image reconstruction.

3. RESULTS

X-ray mammography.

The best x-ray image is presented in Fig. 4a. The phantom was irradiated along the Y-axis. Thickness of the phantom in this direction was 57 mm. The image has a spot (marked with an arrow) in the right upper quarter, which is slightly lighter than the background. This spot corresponds to the sphere #3 with the diameter of 6 mm. All the other spheres were not detected.

Irradiation of the phantom from X- and Z- directions could not provide any images of the spheres, because the thickness of the phantom in these directions was 100 or 97 mm respective, which is beyond sensitivity of the x-ray imaging of the radiologically dense media. Therefore, x-ray radiography could not provide high-contrast images of our phantoms simulating radiologically dense breast with tumors.

Ultrasonography.

Ultrasonography provided better contrast in comparison with x-ray imaging. Fig. 4b represents one of the images obtained from the spheres #3 and #4. The bright line is caused by reflection of acoustic waves from the thread. All the other spheres were out of focus. Bright white spots are caused by noise or artifacts. Therefore, all the gel spheres (from 6-mm to 2-mm in diameter) in the phantom were detectable by ultrasonography. Although the phantoms were designed to simulate acoustically homogenous breast, it was impossible to make the colored spheres with acoustic properties similar to the surrounding gel.

Laser optoacoustic imaging.

The same phantom was used for optoacoustic experiments. Pressure profiles obtained upon irradiation of the spheres #6 and #5 from Z1 and Y2 sides of the phantom are presented in Fig. 5a, 5b. Upper x-axis represents depth, z_v, from the irradiated surface. The sharp edge at z_v=0 resulted from reflection of the laser-induced acoustic wave from the gel-air boundary. It indicates the position (location) of the irradiated surface. All the profiles detected from spheres have bipolar N-shaped profiles. These pressure profiles are typical for signals detected from optically thin absorbing spheres. Wavelet-filtered signal is also presented in Fig.5 (a,b). The wavelet denoising provided substantial increase of the signal-to-noise ratio (of up to 1000). Exponential slope representing background optoacoustic pressure was automatically subtracted from the raw experimental signals by the automatic gain control procedure. Since both spheres were on one line with the laser beam and the acoustic transducer, the pressure profile includes signals from both spherical "tumors" (Fig. 5b).

Similar signals were obtained upon irradiation of all the spheres from each side of the phantom. On the basis of these signals, 2D optoacoustic images were plotted. Fig. 6 (c, d) shows optoacoustic images of the spheres #4, 5, and 6 in different planes (slices) obtained upon irradiation of the spheres from Z1 and Y2 sides of the phantom (from the top of images). Since wavelet-filtering yielded significant noise reduction, the optoacoustic images do not have background noise as in case of x-ray and ultrasound images. Both positions and dimensions of the spheres can be measured with high accuracy from the images. However, this first version of image reconstruction algorithm can not provide detailed information about the shape of the phantom "tumors". More sophisticated computer algorithms utilizing larger number of pressure profiles are being developed to obtain more detailed images.

Downloaded From: http://proceedings.spiedigitallibrary.org/ on 07/11/2016 Terms of Use: http://spiedigitallibrary.org/ss/TermsOfUse.aspx

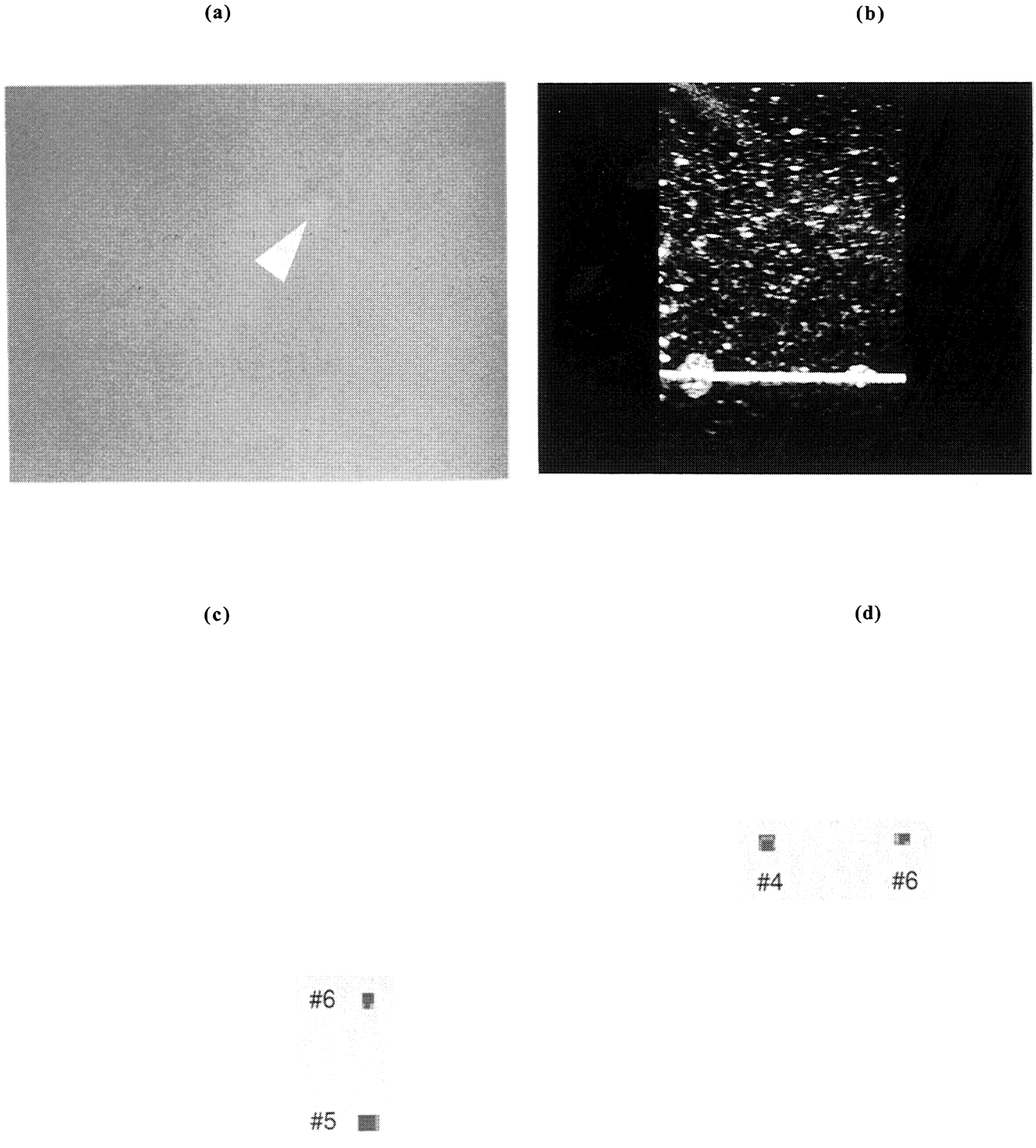

Figure 4. (a) X-ray image of the phantom with a 6-mm sphere; (b) ultrasonic image of the phantom with 2-mm and 6-mm spheres. Optoacoustic images: (c) #5 and # 6 in XY plane; (d) #4 and #6 in ZX plane.

Downloaded From: http://proceedings.spiedigitallibrary.org/ on 07/11/2016 Terms of Use: http://spiedigitallibrary.org/ss/TermsOfUse.aspx

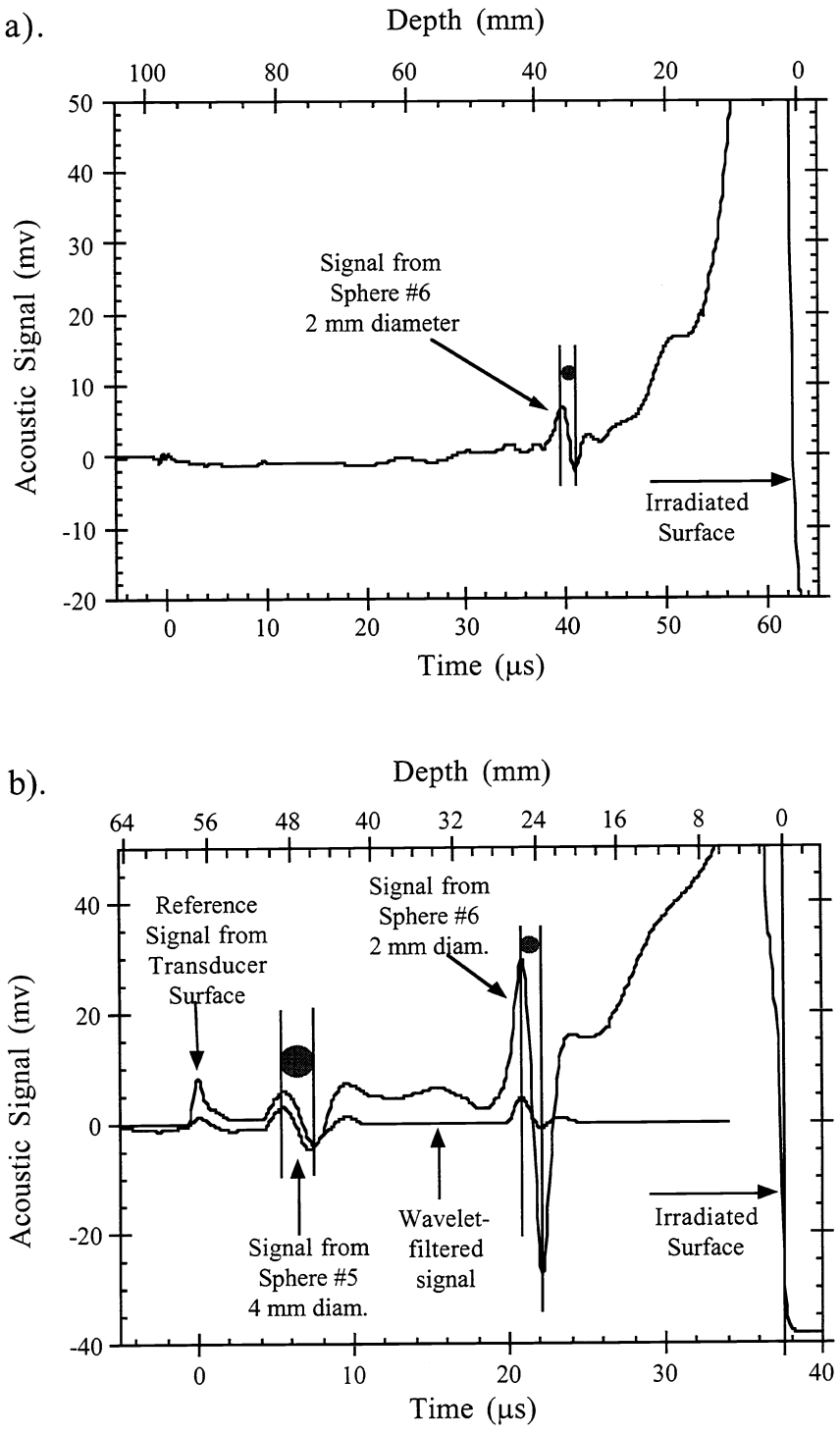

Figure 5. Pressure profiles from the phantom used for the comparative study with signals from the spheres: (a) #6 (Z-1 side of irradiation); (b) #6 and #5 simultaneously (Y-2 side of radiation).

Downloaded From: http://proceedings.spiedigitallibrary.org/ on 07/11/2016 Terms of Use: http://spiedigitallibrary.org/ss/TermsOfUse.aspx

4. DISCUSSION

This comparative study demonstrates that laser optoacoustic imaging can provide images with substantially better contrast than x-ray mammography and ultrasound imaging in case of radiologically dense, acoustically homogenous, but optically inhomogenous phantoms.

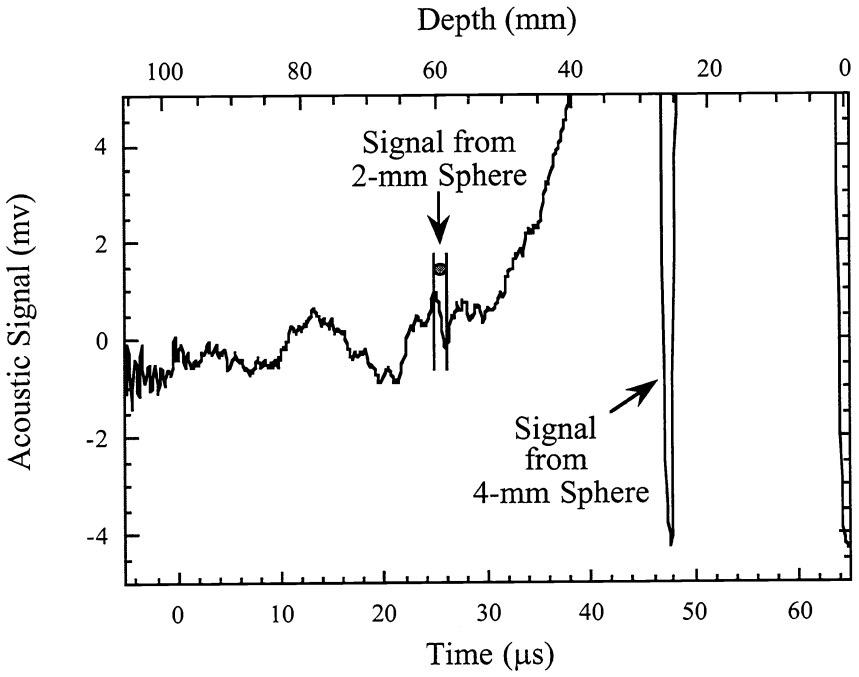

Figure 6. Pressure profile detected from the breast phantom with the 2-mm and 4-mm spheres.

Limits of detection.

Fig. 6 depicts a pressure profile measured from another gel phantom simulating breast with two colored spheres, 2-mm and 4-mm in diameter. All the parameters (optical properties, etc.) of the phantom were similar to that described above. Incident laser fluence was equal to 500 mJ/cm^2. Laser beam diameter was 8 mm.

Signal-to-noise ratio for the pressure pulse from the 2-mm sphere at the depth of 60 mm was approximately two to three. Therefore, one can consider this experiment as the measurement at the limit of detection by our current optoacoustic imaging system. The presence of the 4-mm sphere near the irradiated surface has produced some perturbation of the fluence within the phantom, which made detection of the 2-mm sphere more difficult. However, the real breast pathology is even more complex. The irradiation fluence in our experiment was 5 times higher than that permitted by the National Standard for Safe Use of Lasers [24]. Nevertheless, we used the fluence of 0.5 J/cm^2 to simulate the fluence at the depth of 6 cm that can be achieved with the use of multiple fiberoptic bundles delivering $\leq$ 0.1 J/cm^2 each.

Therefore, the measurement presented in Fig.6 can be used to estimate limits of detection for laser optoacoustic tomography in biological tissues by currently available acoustic transducers. Since the effective light penetration depth estimated as $1/\mu_{eff}$ equaled 1 cm and diameter of laser beam was 0.8 cm, the fluence distribution at high depths ($z>>1/\mu_{eff}$) can be expressed as the following function of the distance from a point source (located close to the irradiated surface) [25,26]:

$$F(z) = AF_o \frac{\exp(-\mu_{eff} z)}{z} \tag{14}$$

where A is the parameter depending on optical properties of irradiated tissue, and F_o is the incident laser fluence.

Downloaded From: http://proceedings.spiedigitallibrary.org/ on 07/11/2016 Terms of Use: http://spiedigitallibrary.org/ss/TermsOfUse.aspx

Combination of formulas (13) and (14) yields the pressure amplitude, P, measured by a transducer as a function of radius of the spherical tumor (acoustic source), the absorption coefficient, the distance between the tumor and the irradiated surface, and parameters (optical and geometrical) of the breast phantom:

$$P_{sph}(\mu_V, z_V, r_0) = \frac{A}{2}\Gamma_V \mu_V F_o \frac{\exp(-\mu_{eff} z_V)}{z_V} \frac{r_0}{D - z_V} \tag{15}$$

where $R_v = D - Z_V$ in this case.

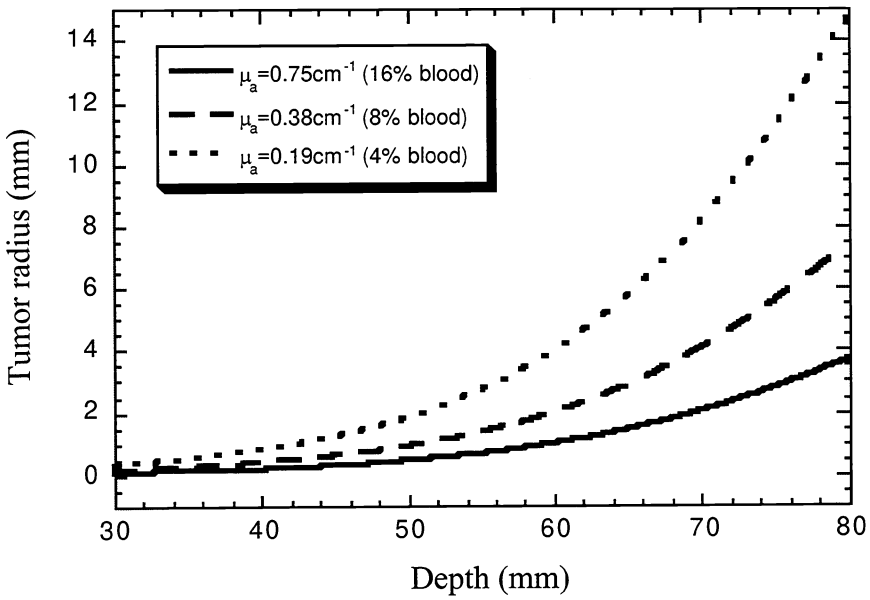

Figure 7. Limit of detection for absorbing spheres in the breast phantoms as a function of depth for different absorption coefficients in "tumors".

Using this formula, one can calculate sensitivity limits for the optoacoustic imaging system as a function of tumor absorption coefficient and the depth of tumor location. Since each acoustic transducer has certain sensitivity and internal electric noise, it can not detect pressure below certain minimal pressure, P_{min}. Substituting P_{min} instead of P in the formula (13), one can get an expression for minimal detectable radius of tumor with an absorption coefficient, μ_V, located at a depth, Z_V, and irradiated with the laser fluence, F_V:

$$r_0 = A' z_V \exp(\mu_{eff} z_V)(D - z_V) \tag{16}$$

where A' is a parameter expressed as:

$$A' = \frac{2P_{min}}{A\Gamma_V \mu_V F_0} \tag{17}$$

The radius of the minimal detectable spherical tumor is plotted with the use of formula (16) in Fig. 7 for three different absorption coefficients. The area above the curves represents experimental parameters for which "tumors" can be detected in the breast phantom. The areas under the curves represent areas below the limits of detection for the transducers used in our experiments.

Downloaded From: http://proceedings.spiedigitallibrary.org/ on 07/11/2016 Terms of Use: http://spiedigitallibrary.org/ss/TermsOfUse.aspx

The Grüneisen coefficient of tissue depends on tissue temperature (the thermomechanical parameters involved with the formula (2) are functions of temperature). The values of Grüneisen coefficient for water calculated with the use of tabular data [26] equal to 0.1 and 0.2 at the temperature of 20 ^{0}C and 37 ^{0}C, respectively. The average value of the Grüneisen coefficient for soft tissues calculated from the data [27,28] is about 4 times higher than that for water. The Grüneisen coefficients are ~ 0.1 for the 10% gelatin used in the experiments at room temperature and ~0.8 for tumor tissue at 37 ^{0}C *in vivo* . Therefore, one can conclude that the available acoustic transducers are sufficiently sensitive to detect 2-mm spherical tumors with absorption coefficient of 0.38 cm^{-1} (8%-blood content) located at the depth of 60 mm in the breast irradiated with the incident laser fluence of 125 mJ/cm^2.

Maximal permissible laser exposure for the skin at λ = 1064 nm equals 100 mJ/cm^2 according to ANSI [24]. Therefore, the current laser optoacoustic imaging system is potentially capable of detecting small tumors at the safe level of laser irradiation. The limits of detection for laser optoacoustic tomography can be further improved with the use of the state-of-the-art electronics and software.

5. CONCLUSION

Our study demonstrated capabilities of laser optoacoustic tomography in detection of mm-size volumes with absorption equal to the absorption of 10% blood at the depth of 5-6 centimeters in phantoms resembling optical properties of breast tissues. Thus, the laser optoacoustic tomography has a potential for early diagnosis of breast tumors. Because modern medical diagnostic techniques have limitations in detection of small tumors (with a volume of $\leq$ 4 mm^3) located at depths of 5-6 centimeters, the laser optoacoustic imaging may occupy a significant niche in diagnosis of breast tumors, especially in radiologically dense and acoustically homogenous breasts.

6. ACKNOWLEDGMENTS

This work was supported by Science Brothers Incorporated, Houston, Texas and the Department of Energy Center of Excellence for Biomedical Applications of Lasers.

7. REFERENCES

1. "Optical Tomography, Photon Migration, and Spectroscopy of Tissue and Model Media: Theory, Human Studies, and Instrumentation," *Proc. SPIE* **2389**, 1995; "Optical Tomography and Spectroscopy of Tissue: Theory, Instrumentation, Model and Human Studies," *Proc. SPIE* **2979**, 1997.
2. *"OSA Proceedings on Advances in Optical Imaging and Photon Migration,"* (R.R. Alfano, ed.), **21**, 1994; *"OSA Trends in Optics and Photonics on Advances in Optical Imaging and Photon Migration,"* R.R. Alfano and J.G. Fujimoto, eds. (OSA, Washington, DC), **2**, 1996.
3. B.J. Tromberg, O. Coquoz, J.B. Fishkin, E.R. Anderson, D. Pham, M. Brenner, and L.O. Svaasand. "Frequency-Domain Photon Migration (FDPM) Measurements of Normal and Malignant Cell and Tissue Optical Properties", In: *"OSA Trends in Optics and Photonics on Biomedical Optical Spectroscopy and Diagnostics"*, ed. by E. Sevic-Muraca and D. Benaron, (OSA, Washington, DC), **3**, pp. 111-116, 1996.
4. J. Folkman. "What is the evidence that tumors are angiogenesis dependent?" *J. Natl. Cancer Inst.*, **82(1)**, pp. 4-6, 1990.
5. N. Weidner, J.P. Semple, W.R. Welch, and J. Folkman. "Tumor angiogenesis and metastasis - correlation in invasive breast carcinoma", *New Engl. J. of Med.*, **324**, pp. 1-7, 1991.
6. A.J. Welch and M. J.C. van Gemert "Optical-Thermal Response of Laser-Irradiated Tissue", eds. Plenum Press, NY, 1995.
7. S. Wray, M. Cope, D.T. Deply, J.S. Wyatt, and E.O.R. Reynolds. "Characterization of the near infrared absorption spectra of cytochrome aa_3 and hemoglobin for the non-invasive monitoring of cerebral oxygenation", *Biochim. et Biophys. Acta*, **933**, pp. 184-192, 1988.
8. K. Leggett. "Optical mammography offers promise as alternative to x-ray detection", *Biophotonics International* , **3(1)**, pp. 56-57, 1996.
9. S.B. Abrams. "Laser-based breast imager competes with x-rays", *Biophotonics International* , **4(1)**, pp. 21-22, 1997.
10. Oraevsky, A.A., S.L. Jacques, F.K. Tittel: Determination of tissue optical properties by time-resolved detection of laser-induced stress waves. *Proc. SPIE* 1993; **1882**: 86-101.
11. R. A. Kruger, P. Liu, "Photoacoustic ultrasound: Pulse production and detection in 0.5% Liposyn", *Medical Physics*, Vol. 21(7), pp. 1179-1184, 1994.

Downloaded From: http://proceedings.spiedigitallibrary.org/ on 07/11/2016 Terms of Use: http://spiedigitallibrary.org/ss/TermsOfUse.aspx

12. A.A. Oraevsky, S.L. Jacques, R.O. Esenaliev, and F.K. Tittel. "Time-Resolved Optoacoustic Imaging in Layered Biological Tissues", In: *"OSA Proceedings on Advances in Optical Imaging and Photon Migration"* , ed. by R. R. Alfano, Academic Press, **21**, pp. 161-165, 1994.
13. A.A. Oraevsky, R.O. Esenaliev, S. L. Jacques, F.K. Tittel, and D. Medina. "Breast Cancer Diagnostics by Laser Opto-Acoustic Tomography", *OSA Trends in Optics and Photonics on Advances in Optical Imaging and Photon Migration,"* R. R. Alfano and J. G. Fujimoto, eds. (OSA, Washington, DC), **2**, pp. 316-321, 1996.
14. A.A. Oraevsky, R.O. Esenaliev, S. L. Jacques, and F.K. Tittel. "Lateral and z-axial resolution in laser optoacoustic imaging with ultrasonic transducers", *Proc. SPIE*, **2389**, pp. 198-208, 1995.
15. A.A Oraevsky, R.O. Esenaliev, S.L. Jacques, and F.K. Tittel. "Laser Opto-Acoustic Tomography for medical diagnostics: principles", *Proc. SPIE* **2676**, pp. 22-31, 1996.
16. R.O. Esenaliev, A.A. Oraevsky, S.L. Jacques, and F.K Tittel. "Laser opto-acoustic tomography for medical diagnostics: Experiments on biological tissues", *Proc. SPIE* **2676**, pp. 84-90, 1996.
17. Oraevsky, A.A., S.L. Jacques, F.K. Tittel: Measurement of tissue optical properties by time-resolved detection of laser-induced transient stress, *Applied Optics,* 1997; **36**(1): 402-415.
18. V.E. Gusev and A.A. Karabutov: "Laser Optoacoustics", AIP Press, New York, 1993.
19. G.J. Diebold and T. Sun. "Properties of optoacoustic waves in one, two, and three dimensions", *Acustica*, **80**, pp. 339-351, 1994.
20. G.M. Hale and M.R. Querry: "Optical constants of water in the 200-nm to 200-μm wavelength region", *Appl. Optics*, **12**, pp. 555-563, 1973.
21. J. Kolzer, G. Mitic, J. Otto, and W. Zinth: "Measurements of the optical properties of breast tissue using time resolved transillumination", *Proc. SPIE* **2326**, pp. 143-152, 1994.
22. K. Suzuki, Y. Yamashita, K. Ohta, M. Kaneko, M. Yoshida, and B. Chance. "Quantitative measurement of optical parameters in normal breasts using time-resolved spectroscopy: *in vivo* results of 30 Japanese women", *J. Biomed. Optics,* **1(3)**, pp. 330-334, 1996.
23. D. Donoho: "De-noising by Soft-Thresholding", IEEE Trans. Info. Theory, **41**(3): 613-627, 1995.
24. "American National Standard for Safe Use of Lasers", ANSI Z136.1-1993.
25. T.J. Farrell, M.S. Patterson, and B.C. Wilson. "A diffusion theory model of spatially resolved, steady state diffuse reflectance for the noninvasive determination of tissue optical properties in vivo", *Med. Phys.*, **19**, pp. 879-888, 1992.
26. R.S. Haskell, L.O. Svaasand, Tsong-Tseh Tsay, Tu-Chen Feng, M.S. McAdams, and B.J. Tromberg. "Boundary conditions for the diffusion equation in radiative transfer", *J. Opt. Soc. Am. A*, **11**, pp. 2727-2741, 1994.
27. Handbook of Chemistry and Physics. 66th Ed. 1986.
28. S.A. Goss, R.L. Johnston, and F. Dunn: "Comprehensive compilation of empirical ultrasonic properties of mammalian tissues", *J. Acoust. Soc. Am.*, **64(2)**, pp. 423-457, 1978.
29. F.A. Duck, "*Physical properties of tissue: A comprehensive reference book*", Academic Press, San Diego, 1990.

Downloaded From: http://proceedings.spiedigitallibrary.org/ on 07/11/2016 Terms of Use: http://spiedigitallibrary.org/ss/TermsOfUse.aspx